NASA / CR-2001-210837

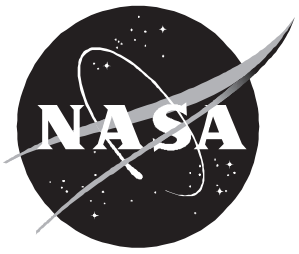

Evaluation of CFD Turbulent Heating Prediction Techniques and Comparison With Hypersonic Experimental Data

Arthur D. Dilley
Swales Aerospace, Hampton, Virginia

March 2001

The NASA STI Program Office . . . in Profile

Since its founding, NASA has been dedicated to the advancement of aeronautics and space science. The NASA Scientific and Technical Information (STI) Program Office plays a key part in helping NASA maintain this important role.

The NASA STI Program Office is operated by Langley Research Center, the lead center for NASA's scientific and technical information. The NASA STI Program Office provides access to the NASA STI Database, the largest collection of aeronautical and space science STI in the world. The Program Office is also NASA's institutional mechanism for disseminating the results of its research and development activities. These results are published by NASA in the NASA STI Report Series, which includes the following report types:

- TECHNICAL PUBLICATION. Reports of completed research or a major significant phase of research that present the results of NASA programs and include extensive data or theoretical analysis. Includes compilations of significant scientific and technical data and information deemed to be of continuing reference value. NASA counterpart of peer-reviewed formal professional papers, but having less stringent limitations on manuscript length and extent of graphic presentations.

- TECHNICAL MEMORANDUM. Scientific and technical findings that are preliminary or of specialized interest, e.g., quick release reports, working papers, and bibliographies that contain minimal annotation. Does not contain extensive analysis.

- CONTRACTOR REPORT. Scientific and technical findings by NASA-sponsored contractors and grantees.

- CONFERENCE PUBLICATION. Collected papers from scientific and technical conferences, symposia, seminars, or other meetings sponsored or co-sponsored by NASA.

- SPECIAL PUBLICATION. Scientific, technical, or historical information from NASA programs, projects, and missions, often concerned with subjects having substantial public interest.

- TECHNICAL TRANSLATION. English-language translations of foreign scientific and technical material pertinent to NASA's mission.

Specialized services that complement the STI Program Office's diverse offerings include creating custom thesauri, building customized databases, organizing and publishing research results . . . even providing videos.

For more information about the NASA STI Program Office, see the following:

- Access the NASA STI Program Home Page at *http://www.sti.nasa.gov*

- Email your question via the Internet to help@sti.nasa.gov

- Fax your question to the NASA STI Help Desk at (301) 621-0134

- Telephone the NASA STI Help Desk at (301) 621-0390

- Write to:
  NASA STI Help Desk
  NASA Center for AeroSpace Information
  7121 Standard Drive
  Hanover, MD 21076-1320

NASA / CR-2001-210837

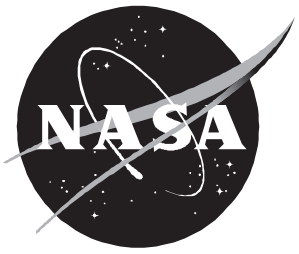

Evaluation of CFD Turbulent Heating Prediction Techniques and Comparison With Hypersonic Experimental Data

Arthur D. Dilley
Swales Aerospace, Hampton, Virginia

National Aeronautics and
Space Administration

Langley Research Center
Hampton, Virginia 23681-2199

Prepared for Langley Research Center
under Contract NAS1-00135

March 2001

Acknowledgments

This work was performed under contracts NAS1-19864, NAS1-96013 and NAS1-00135 for NASA Langley Research Center. This report summarizes the CFD portion of a larger effort to assess the accuracy of turbulent cold wall heating predictions for hypersonic vehicles. The author would like to thank the other participants in this study, Abel Torres and Zane Pinckney, for their assistance in this CFD analysis. The advise and assistance of Ricky Thompson, Paul Vitt, Bob Bittner and Joseph Morrison are also greatly appreciated. The author would also like to recognize and thank Dr. Julius Harris for his suggestion to try local damping with the Baldwin-Lomax turbulence model in CFL3DE and Dr. Clay Anderson for his encouragement and support.

Available from:

NASA Center for AeroSpace Information (CASI)
7121 Standard Drive
Hanover, MD 21076-1320
(301) 621-0390

National Technical Information Service (NTIS)
5285 Port Royal Road
Springfield, VA 22161-2171
(703) 605-6000

Abstract

Results from a study to assess the accuracy of turbulent heating and skin friction prediction techniques for hypersonic applications are presented. The study uses the original and a modified Baldwin-Lomax turbulence model with a space marching code. Grid converged turbulent predictions using the wall damping formulation (original model) and local damping formulation (modified model) are compared with experimental data for several flat plates. The wall damping and local damping results are similar for hot wall conditions, but differ significantly for cold walls, i.e. $T_w / T_t < 0.3$, with the wall damping heating and skin friction 10-30% above the local damping results. Furthermore, the local damping predictions have reasonable or good agreement with the experimental heating data for all cases. The impact of the two formulations on the van Driest damping function and the turbulent eddy viscosity distribution for a cold wall case indicate the importance of including temperature gradient effects. Grid requirements for accurate turbulent heating predictions are also studied. These results indicate that a cell Reynolds number of 1 is required for grid converged heating predictions, but coarser grids with a y^+ less than 2 are adequate for design of hypersonic vehicles. Based on the results of this study, it is recommended that the local damping formulation be used with the Baldwin-Lomax and Cebeci-Smith turbulence models in design and analysis of Hyper-X and future hypersonic vehicles.

1. Introduction

NASA's Hyper-X Program was initiated to mature hypersonic air-breathing propulsion, and the design and analysis tools required to build an efficient hypersonic cruise vehicle[1]. The Hyper-X program will conduct flight tests of an airframe integrated scramjet at Mach numbers of 7 and 10. Successful demonstration of acceleration at Mach 7 and sustained cruise at Mach 10 will move hypersonic air-breathing vehicle technology from the laboratory into the flight environment. The Hyper-X vehicle is designed to have turbulent flow over a significant portion of the scramjet engine flowpath. The vehicle structure must be designed to survive the increased heating due to this turbulent flow, while the overall thrust predictions must consider the increased skin friction. This connection between the turbulent heating and skin friction predictions, and the vehicle design raised concerns regarding the accuracy of turbulent flow prediction techniques. To address these concerns, a study to assess the accuracy of the turbulent heating and skin friction prediction techniques used to design the Hyper-X vehicle was undertaken. This study considered both analytical and engineering methods, and Computational Fluid Dynamics (CFD) codes. The CFD results from the study are presented in this report.

In this study, an upwind, finite volume flow solver, CFL3DE[2], was used to evaluate the accuracy of the Baldwin-Lomax algebraic turbulence model[3] for hypersonic applications. Shirazi and Truman[4], and Vuong and Coakley[5] have previously compared predictions using the Baldwin-Lomax model with experimental data for hypersonic flows. However, the wall conditions considered in this study are significantly colder than those from the previous studies and span the expected range for the Mach 7 and Mach 10 Hyper-X flights. In the present study, grid converged heating and skin friction predictions for flat plates at Mach numbers from 6 to 9 were compared with experimental measurements to determine the accuracy of the predictions. In some cases, the CFD solutions significantly overpredicted the turbulent heating levels. In an effort to improve the agreement, a modification to the algebraic turbulence model was incorporated into the CFD code. This modification involved a small

change to the model, but had a large impact on the accuracy of the predictions. The modification to the turbulence model and its impact on the heating and skin friction predictions are discussed. Also, an assessment of the computational accuracy requirements for turbulent heating predictions during vehicle design activities is presented. Some recommendations for future design and analysis of hypersonic vehicles are also given.

2. Turbulence Modeling

Some of the computational tools used in the design of hypersonic vehicles utilize algebraic turbulence models to simulate the effects of turbulence. These algebraic models are easily incorporated into CFD codes and require the solution of no additional equations. The Baldwin-Lomax model is patterned after the Cebeci-Smith turbulence model[6]. With merged inviscid-viscous flowfields, determining the boundary layer edge can be difficult. To avoid this difficulty, the Baldwin-Lomax model is normally used in Parabolized Navier-Stokes (PNS) and Navier-Stokes (NS) flow solvers.

The Baldwin-Lomax algebraic turbulence model uses an inner and outer layer formulation. In the inner layer, the turbulent eddy viscosity, μ_t, is given by

$$(\mu_t)_{inner} = \rho(\kappa y D)^2 |\omega| \ , \tag{1}$$

where ρ is the density, κ is the von Karman constant, y is the local distance normal to the body surface and $|\omega|$ is the magnitude of the local vorticity vector. The van Driest damping function, D, is given by

$$D = 1 - \exp\left(\frac{-y^+}{A^+}\right), \tag{2}$$

where A^+ is a constant and y^+ is given by

$$y^+ = \frac{\sqrt{\rho_w \tau_w}\, y}{\mu_w}, \tag{3}$$

where ρ_w is the density at the wall, μ_w is the laminar viscosity at the wall and τ_w is the wall shear stress. In the outer layer, the turbulent eddy viscosity is given by

$$(\mu_t)_{outer} = KC_{cp}\rho F_{wake} F_{Kleb}(y), \tag{4}$$

where K is the Clauser constant and C_{cp} is an additional constant. For wall bounded shear flows, F_{wake} is given by

$$F_{wake} = y_{max} F_{max}, \tag{5}$$

where y_{max} and F_{max} correspond to the location of the maximum value of the "vorticity" function,

$$F(y) = y|\omega|D \ . \tag{6}$$

The Klebanoff intermittency factor is given by

$$F_{Kleb}(y) = 1 \Big/ \left[1 + 5.5\left(\frac{C_{Kleb}\, y}{y_{max}}\right)^6\right] \ , \tag{7}$$

where C_{Kleb} is a constant. The constants in the model have the following values

$$A^+=26.$$
$$C_{cp}=1.6$$
$$C_{Kleb}=0.3$$
$$\kappa=0.4$$
$$K=0.0180.$$

The turbulent eddy viscosity becomes

$$\mu_t = \begin{pmatrix} (\mu_t)_{inner}, y \le y_{cross} \\ (\mu_t)_{outer}, y > y_{cross} \end{pmatrix}, \tag{8}$$

where y_{cross} is the smallest value of y at which the inner layer and outer layer formulations for the turbulent eddy viscosity are equal.

The inner layer of the Cebeci-Smith model is similar to eq. [1], but the magnitude of the vorticity is replaced with the normal gradient of the tangential velocity. In the boundary layer, these two quantities are similar. Also, the Cebeci-Smith model uses a different definition for y^+ with

$$y^+ = \frac{\sqrt{\rho\tau_w}y}{\mu}, \tag{9}$$

where ρ and μ are local values of density and laminar viscosity, respectively. The two definitions of y^+, eq.[3] and eq.[9], differ by the factor

$$Y = \sqrt{\frac{\rho}{\rho_w}} \cdot \frac{\mu_w}{\mu}. \tag{10}$$

This factor becomes significant in cold wall boundary layers, where the temperature gradient at the surface is large. To determine the effect of this factor, the Baldwin-Lomax model in CFL3DE was modified to use eq. [9] in place of eq. [3]. Using the two definitions for y^+ as guidelines, the van Driest damping function, eq. [2], with eq. [3] for y^+ is defined as "wall damping" and with eq. [9] as "local damping." An examination of several papers on turbulence modeling for high speed flows has shown inconsistencies in the manner in which y^+ is defined with these two algebraic turbulence models. For example, Voung and Coakley[5], and Stock and Haase[7] use wall damping with both the Cebeci-Smith and Baldwin-Lomax models, while Shirazi and Truman[4] use wall damping for Baldwin-Lomax and local damping for Cebeci-Smith. Cheatwood and Thompson[8] use local damping for both turbulence models. There appears to be some confusion as to which y^+ definition should be used in these algebraic turbulence models. Therefore, heating and skin friction predictions using both definitions for y^+ are presented in this report. The results will be used to recommend guidelines for applying the Baldwin-Lomax turbulence model to hypersonic flows.

3. Grid Refinement

Grid refinement was used in this study to evaluate the effect of grid resolution on turbulent heating and skin friction predictions, and to obtain grid converged solutions for comparison with the experimental data. The grid refinement was performed in both the axial and normal directions. The normal grid was created using the grid distribution method of Cheatwood and

Thompson[8]. This distribution clusters the grid points to adequately resolve the boundary layer gradients without overly resolving the outer shock region. Therefore, grid stretching is used near the surface and a uniform spacing is used in the outer region of the grid. At the interface of these regions, the grid spacings are forced to match. The fraction of the total cells in the stretched region is given by

$$F_{str} = \max[\frac{1}{2}, 1 - \frac{32}{J}], \tag{11}$$

where J is the total number of normal cells. The number of stretched cells then becomes

$$J_{str} = F_{str} J. \tag{12}$$

A sinusoidal distribution is used in the recursive formula for the nondimensional height of the stretched cells and is given by

$$\Delta\tilde{y}_j = \left\{1 + f_{str}\sin\left[\frac{(j-1)\pi}{J_{str}-1}\right]\right\}\Delta\tilde{y}_{j-1}, \tag{13}$$

where f_{str} is iteratively determined. The total nondimensional distance from the surface to the outer edge of a cell is given by

$$\tilde{y}_j = \sum_{i=1}^{j} \Delta\tilde{y}_i. \tag{14}$$

In these calculations, the height of the first cell and the outer boundary are specified. An iterative procedure is then used to compute the value of f_{str} which yields a nondimensional distance from the surface to the outer boundary of 1. Dimensionality is returned using

$$y_j = \tilde{y}_j y_{standoff}, \tag{15}$$

where $y_{standoff}$ is the physical distance between the surface and the outer boundary. This type of normal grid distribution is well suited for a grid refinement study involving surface quantities like heat transfer and skin friction. With relatively small increases in the total number of normal grid points, the grid near the surface can be refined as needed, while an adequate uniform spacing in the outer region remains relatively unchanged.

The axial grid starts slightly downstream of the leading edge of the flat plate, with the axial grid step growing by a factor of 1.03 until a specified maximum axial step is reached. During the grid refinement, the first axial plane is moved forward and the maximum axial step is reduced.

Cheatwood and Thompson[8], and Weilmuenster and Gnoffo[9] recommend a cell Reynolds number of 1 for turbulent calculations, with the cell Reynolds number defined as

$$Re_{cell} = \frac{\rho_1 a_1 \Delta y_1}{\mu_1}, \tag{16}$$

where ρ_1, a_1 and μ_1 are the density, speed of sound and laminar viscosity, respectively, at the first cell and Δy_1 is the cell height. However, the standard measure of grid resolution for viscous flows uses the value of y^+ at the first point off the surface. To accurately resolve the

temperature profile, Fletcher[10] recommends a y^+ less than 2. The grid refinement study will address the required cell Reynolds number and y^+ for efficient and accurate turbulent heating and skin friction predictions.

4. Computational Procedure

Previous studies using this upwind, finite volume flow solver have demonstrated its ability to accurately predict the flowfield on sharp cones[11], sharp nose hypersonic forebodies[12] and hypersonic forebody/inlet flowpaths[13,14]. Results with grid refinement have shown reasonable agreement with experimental heat transfer measurements on forebodies at Mach numbers from 11 to 19 [13,14].

The PNS solution was started using conical flow at the first axial station. This required that the normal grid points in the first cell extrapolate to the leading edge of the flat plate, with the first cell located slightly downstream of the leading edge, as shown in Figure 1. After a conical solution was obtained, the marching solution was initiated. The grid was constructed with the outer boundary located to capture the Mach line originating from the nose of the flat plate.

Transition to turbulence was calculated using the exponential streamwise intermittency function of Dhawan and Narasimha[15], with the onset and end of transition based upon the experimental data. Turbulent flow was modeled using the original and modified Baldwin-Lomax model as discussed previously.

Solutions were considered to be grid converged when the heat transfer and skin friction distributions were unchanged with further grid refinement. Grid converged solutions were first obtained using local damping and then, wall damping solutions were obtained on the finest grid. Results from a boundary layer code[16] are also presented for reference. The boundary layer code uses the Cebeci-Smith turbulence model with local damping in the van Driest damping function.

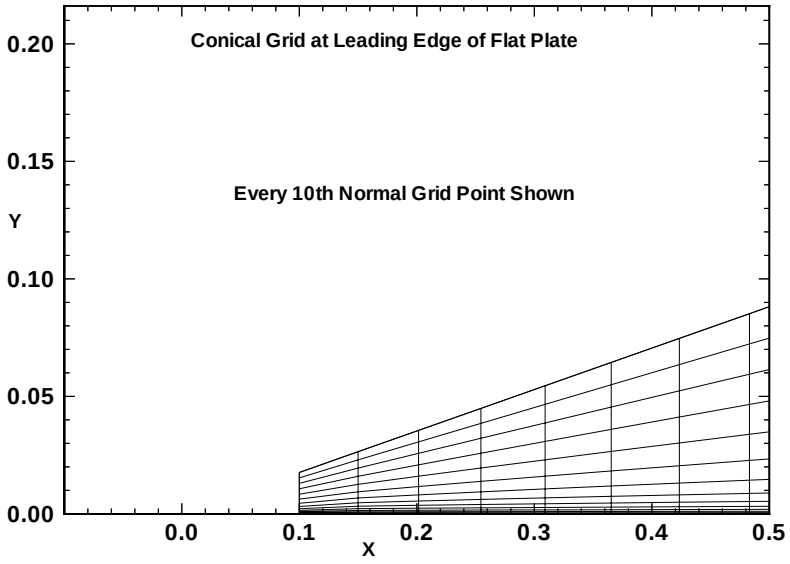

Figure 1. Conical Grid at Nose of Flat Plate

5. Results

5.1 Experimental Database

A large database of experimental heat transfer and skin friction measurements on simple configurations is available for assessing the accuracy of hypersonic turbulent flow prediction techniques. The data covers a wide range of wall conditions. The expected wall temperatures on the Mach 7 and Mach 10 flight vehicles vary with the tungsten forebody as low as 1000^{o} R and the thermal protection system (TPS) tiles as high as 2500^{o} R. Relative to the flight total temperatures, these wall temperatures are rather cold. For purposes of this study, a cold wall is defined as having a T_w / T_t less than 0.3, where T_w is the wall temperature and T_t is the freestream total temperature. The majority of the results presented in this report are for cold walls. The experimental datasets are from Bertram, Cary and Whitehead[17]; Bertram and Neal[18]; and Wallace[19]. The flow conditions for all the cases are given in Table 1. The Bertram, Cary and Whitehead, and Bertram and Neal datasets are from Mach 6 flat plate experiments conducted in the 20-Inch hypersonic tunnel at NASA Langley Research Center. The data consist of Stanton number distributions. One of the cases has a cold wall, while the remaining cases are near adiabatic wall conditions. Also, one of the cases has the flat plate oriented at an angle of attack of 15^{o}. The Wallace flat plate data covers a Mach number range from 6.4 to 8.8. All of the cases have a cold wall, with a total enthalpy ratio, H_w / H_t,varying from 0.11 to 0.26. With the perfect gas assumption from the experiments, the total enthalpy ratio, H_w / H_t, is equivalent to the temperature ratio, T_w / T_t. The data consist of Stanton number and skin friction coefficient distributions. The three Wallace cases considered in this study provide a good sampling of the range of Mach number and wall temperature from the Wallace dataset. The range of wall conditions from these experimental datasets span the expected wall conditions from the Hyper-X flights ($0.11 < T_w / T_t < 0.57$).

Table 1. Flow Conditions for Flat Plate Cases

Reference	Case Description	M_∞	T_∞ (K)	Re_∞ (1/m)	T_w (K)	Data
Bertram, Cary and Whitehead[17]	$T_w / T_t = 0.2$	6.0	65.04	26.38×10^6	106.67	N_{st}
	$T_w / T_t = 0.6$	6.0	65.04	26.38×10^6	320.0	N_{st}
Bertram and Neal[18]	$T_w / T_t = 0.65$ $\alpha = 0.0^o$	6.0	63.01	26.38×10^6	335.84	N_{st}
	$T_w / T_t = 0.65$ $\alpha = 15.0^o$	6.0	63.01	26.38×10^6	335.84	N_{st}
Wallace[19]	$H_w / H_t = 0.11$	7.12	240.0	16.05×10^6	299.0	N_{st}
	$H_w / H_t = 0.19$	8.80	93.99	60.21×10^6	296.3	N_{st}, C_f
	$H_w / H_t = 0.26$	7.00	105.0	84.64×10^6	296.0	N_{st}, C_f

5.2 Mach 6 Cases

The grid dimensions and spacings, and transition onset and end locations for the Mach 6 cases are given in Table 2. The grid converged solution is with grid 1 and the finest grid considered is grid 2. The Re_{cell} and y^+ for each grid are also given. In some instances, the maximum axial grid spacing, Δx_{max}, was not changed when the normal grid was refined. Only heat transfer measurements were reported for the Mach 6 flat plate tests with the experimental data consisting of Stanton number distributions, where the measured heat transfer has been normalized using the edge conditions. For the angle of attack case, the edge conditions are the post-shock conditions, i.e. M_{edge}=4.0, and not the freestream conditions.

Table 2. Mach 6 Cases

Case Description	Grid	Re_{cell}	y_1^+	Grid Dimensions (Normal x Axial)	Δy_1 (in)	Δx_{max} (in)	Transition onset - end
$T_w / T_t = 0.20$	1	2.0	.15	161 x 191	$.38 \times 10^{-4}$	.10	4.8" - 10.4"
	2	1.0	.07	201 x 311	$.19 \times 10^{-4}$	.05	
$T_w / T_t = 0.60$	1	1.0	.07	121 x 191	$.9 \times 10^{-4}$	.10	3.75" - 7.5"
	2	0.5	.03	161 x 191	$.38 \times 10^{-4}$	.10	
$T_w / T_t = 0.65$ $\alpha = 0.0^o$	1	1.0	.07	121 x 191	$.1 \times 10^{-3}$	.10	3.75" - 7.5"
	2	0.4	.03	161 x 191	$.4 \times 10^{-4}$	.10	
$T_w / T_t = 0.65$ $\alpha = 15.0^o$	1	2.5	.13	161 x 191	$.4 \times 10^{-4}$	.10	3.15" - 5.25"
	2	1.0	.05	201 x 301	$.16 \times 10^{-4}$	.06	

The results for the cold wall case, T_w/T_t=0.2, are plotted using the running Reynolds number, R_x, in Figures 2 and 3. Comparisons of CFD and boundary layer heating predictions with experimental data are shown in Figure 2. The skin friction results are shown in Figure 3. The local damping results with grid 2, the finest grid, differ by less than 0.3% from the grid 1 results, indicating the solution is grid converged. The grid 1 and grid 2 solutions have 95 and 120 points in the boundary layer, respectively. The local damping predictions are in reasonable agreement with the data with a Root Mean Square (RMS) deviation of 15% from the turbulent data. The wall damping predictions are about 23% above the local damping results and have an RMS deviation of 41% from the turbulent data. The boundary layer heating and skin friction results are in excellent agreement with the local damping predictions. The

results for the hot wall case, T_w/T_t=0.6, are shown in Figures 4 and 5. Comparisons of CFD and boundary layer heating predictions with experimental data are shown in Figure 4. The skin friction results are shown in Figure 5. The CFD predictions using local and wall damping differ by only 2% and have good agreement with the data with an RMS deviation of 8% from the turbulent data. The boundary layer results are 4% higher than the CFD. The grid 1 and grid 2 solutions have 65 and 94 points in the boundary layer, respectively. These two cases show the effect of wall temperature with the local damping and wall damping formulations of the Baldwin-Lomax turbulence model. For hot walls with small temperature gradients, the two formulations give slightly different results; but for cold walls with large temperature gradients, the results differ significantly. Only the local damping results have good or reasonable agreement with the data for both cases.

Comparisons of CFD and boundary layer heating predictions with experimental data for the other Mach 6 cases are shown in Figures 6 and 7. The 0.0^o angle of attack CFD results in Figure 6 have fair agreement with the data with an RMS deviation of 18% with local damping and 21% with wall damping. The 15.0^o angle of attack CFD results in Figure 7 are plotted using local edge conditions and have good agreement with the data with an RMS deviation of 7% with both local and wall damping. The good agreement at 15.0^o angle of attack and the large overshoot in the 0.0^o angle of attack data at the end of transition suggest a possible tunnel-induced disturbance causing the less than good agreement in Figure 6. For both cases, the boundary layer results were 5% above the CFD predictions. These hot wall CFD results are similar to the previous hot wall case with the two formulations yielding only slight differences.

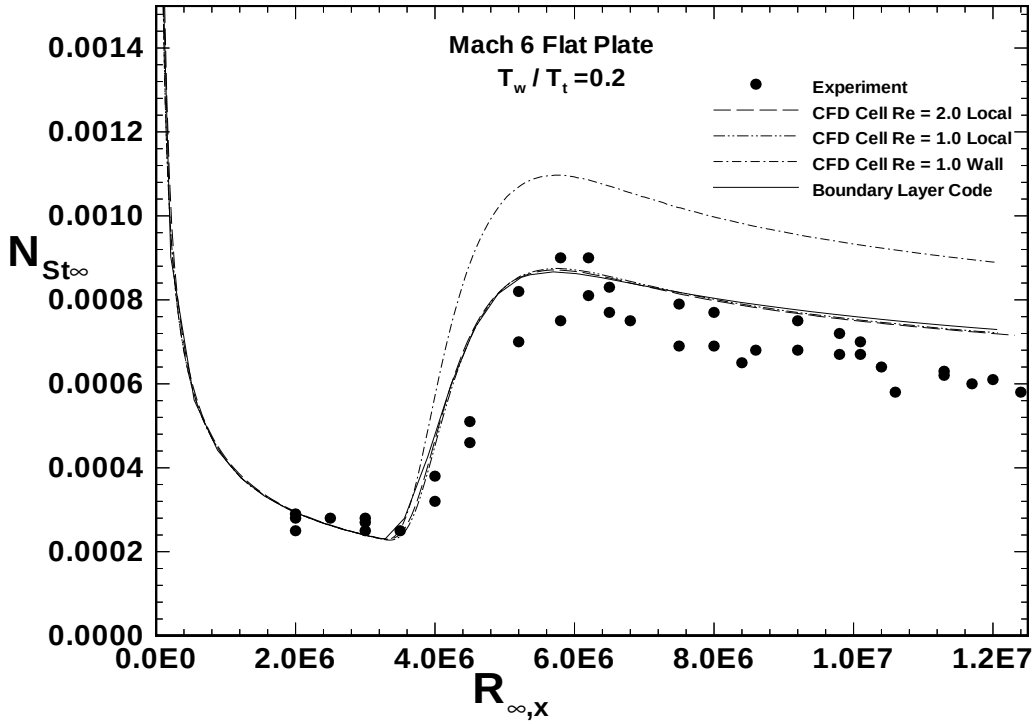

Figure 2. Mach 6 Cold Wall Heating Comparisons

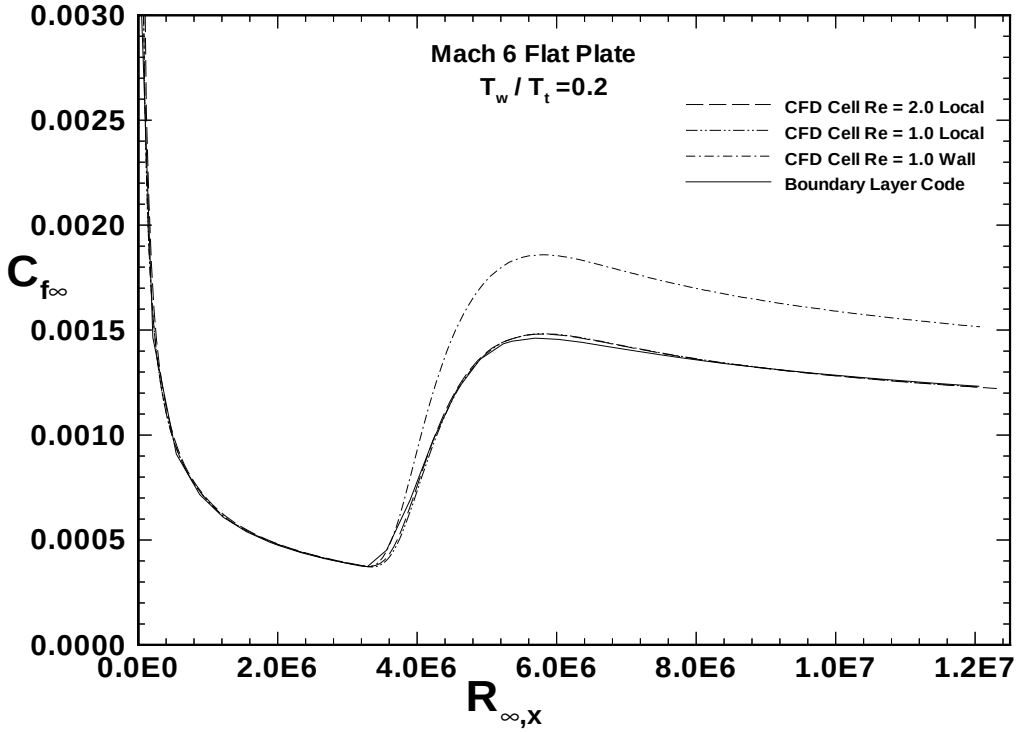

Figure 3. Mach 6 Cold Wall Skin Friction Comparisons

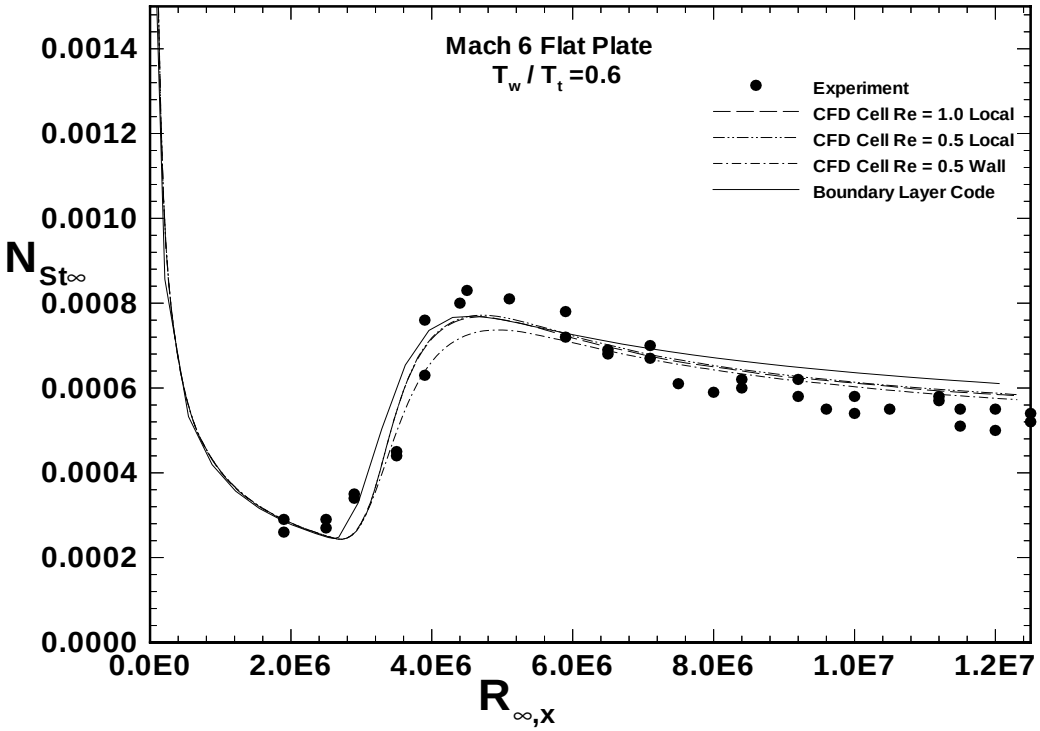

Figure 4. Mach 6 Hot Wall Heating Comparisons

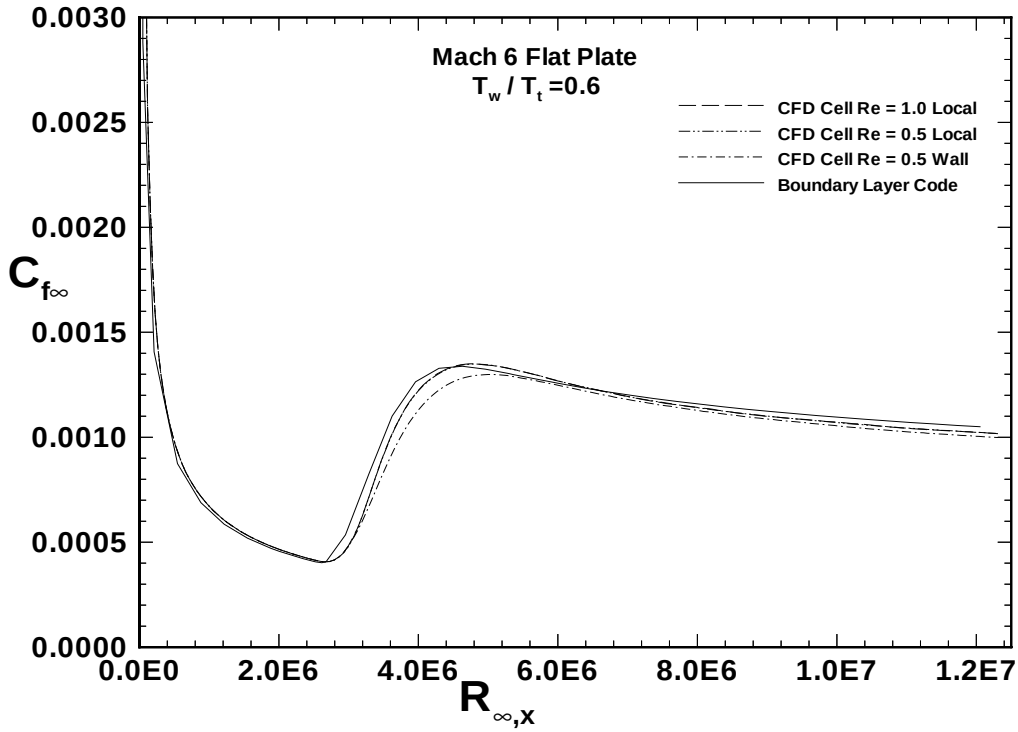

Figure 5. Mach 6 Hot Wall Skin Friction Comparisons

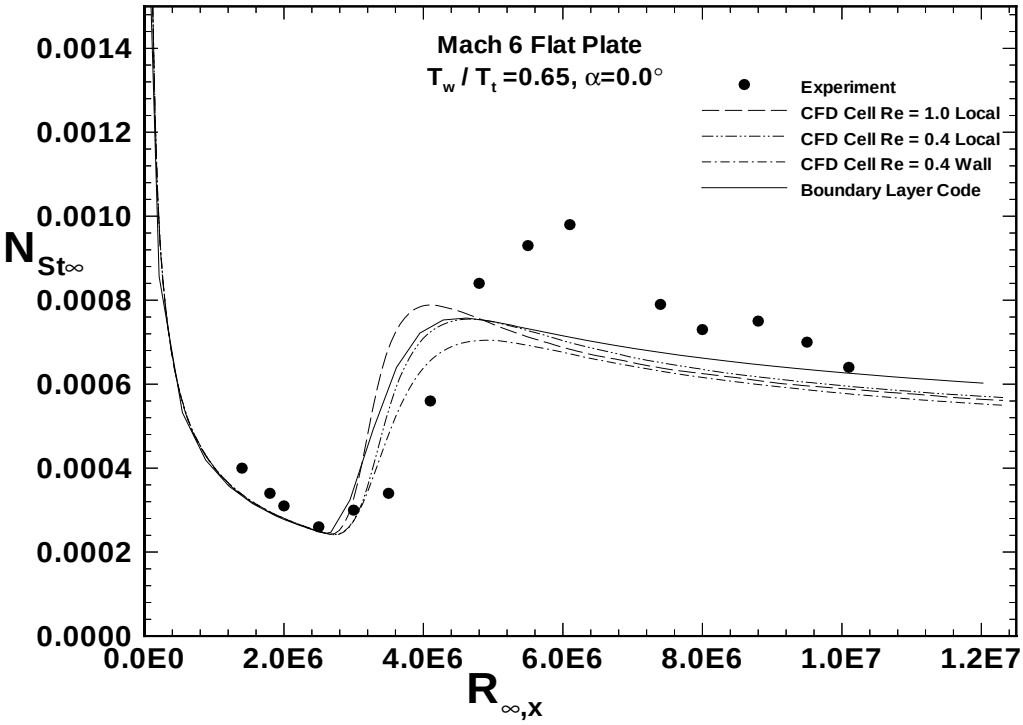

Figure 6. Mach 6 Hot Wall Heating Comparisons

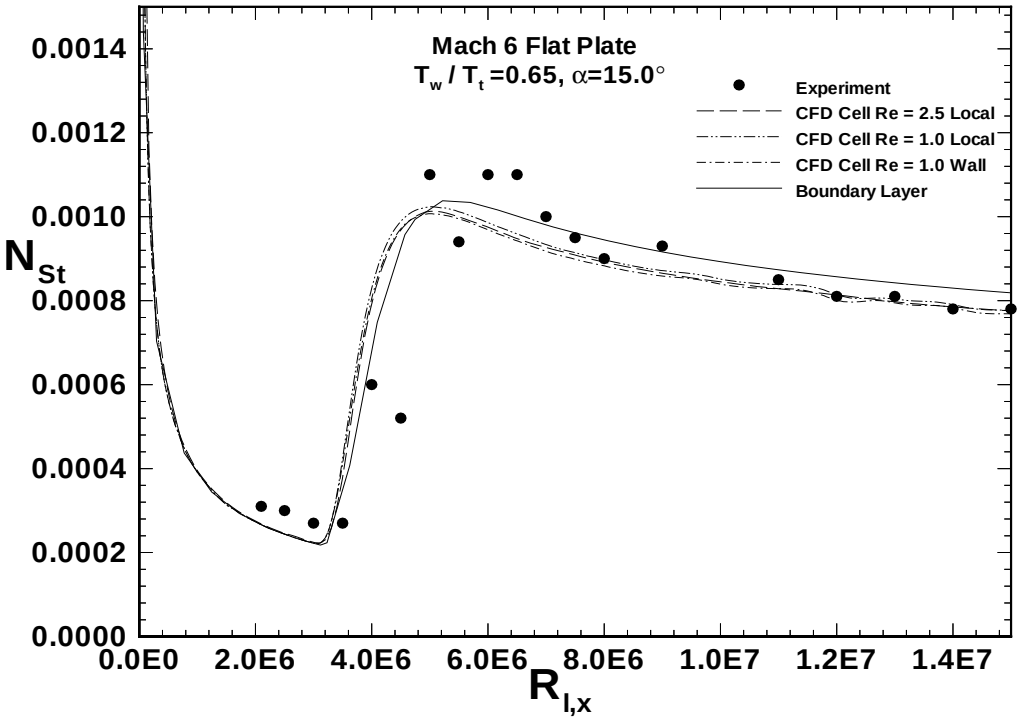

Figure 7. Mach 6 Hot Wall, Angle of Attack Heating Comparisons

5.3 Wallace Cold Wall Cases

The Mach 6 results indicate the turbulent heating predictions with local damping and wall damping differ significantly under cold wall conditions. Because accurate cold wall heating predictions are crucial to the thermal analysis of the Hyper-X flight vehicles and the related TPS sizing, cold wall effects were further studied with several cases from the Wallace dataset[19]. The grid dimensions and spacings, and transition onset and end locations for the Wallace cases are given in Table 3. The Re_{cell} and y^+ for each grid are also given. The experimental data consist of Stanton number and skin friction coefficient distributions, where the measured quantities have been normalized using the edge conditions.

Table 3. Wallace Cold Wall Cases

Case Description	Grid	Re_{cell}	y_1^+	Grid Dimensions (Normal x Axial)	Δy_1 (in)	Δx_{max} (in)	Transition onset - end
Mach 7.12	1	2.2	.18	161 x 211	$.5x10^{-4}$	.15	5.8" - 11.5"
H_w / H_t = 0.11	2	1.0	.08	201 x 321	$.23x10^{-4}$	.10	
Mach 8.80	1	2.2	.17	161 x 211	$.6x10^{-4}$	.15	3.9" - 8.0"
H_w / H_t = 0.19	2	1.0	.08	201 x 321	$.27x10^{-4}$	.10	
Mach 7.00	1	2.3	.15	161 x 211	$.3x10^{-4}$	.15	2.0" - 4.5"
H_w / H_t = 0.26	2	1.0	.07	201 x 321	$.14x10^{-4}$	.10	

The results for the Wallace cases are plotted against the running Reynolds number, R_x, in Figures 8-13. For each case, the grid 1 and grid 2 solutions have 96 and 126 points in the boundary layer, respectively. Comparisons of CFD and boundary layer heating predictions with the Mach 7.12 experimental data are shown in Figure 8. The skin friction results for that case are shown in Figure 9. The local damping predictions have good agreement with the heating data with an RMS deviation of 5%. The wall damping heating and skin friction predictions are 32% above the local damping results and have an RMS deviation of 39% with the heating data. Comparisons of CFD and boundary layer predictions with the Mach 8.80 experimental data are shown in Figures 10 and 11. The local damping predictions have reasonable agreement with the heating data and fair agreement with the skin friction data, with RMS deviations of 11% and 19%, respectively. The wall damping predictions are 19% above the local damping results and have RMS deviations of 31% with the heating data and 40% with the skin friction data. Comparisons of CFD and boundary layer predictions with the Mach 7.0 experimental data are shown in Figures 12 and 13. The local damping predictions have reasonable agreement with the data with RMS deviations of 14% with the heating data and 12% with the friction data. The wall damping predictions are 12% above the local damping results and have RMS deviations of 28% with the heating data and 22% with the friction data. For all cases, the boundary layer results and the local damping predictions are within 3%.

Profiles from the Mach 7.12 solutions at the last axial station have been studied to determine the impact of the two damping formulations on the flowfield properties and the turbulent eddy viscosity distribution. The full temperature profiles are shown in Figure 14, with a blow-up of the region near the surface in Figure 15. The agreement between the local damping solution and the boundary layer results is good through the inner layer region, but they differ somewhat in the outer portion of the boundary layer. This may be attributable to the differences in the modeling of the outer layer region between the Baldwin-Lomax and Cebeci-Smith models. Also, the wall damping solution has a thicker boundary layer than the local damping solution. Figures 14 and 15 have large temperature gradients near the surface, with a peak in temperature at approximately 0.005 inches from the surface. The impact of this temperature gradient on the van Driest damping function, eq. [2], with local damping and wall damping is shown in Figure 16. The damping function with either formulation becomes 1.0 above a height of 0.06 inches, but the damping function's exponential term decays significantly slower with local damping. The turbulent eddy viscosity profiles near the surface are shown in Figure 17. A slower initial growth in μ_t is present with local damping due to the increased damping in the first 0.06 inches shown in Figure 16. The turbulent eddy viscosity profiles in the inner and outer layers are shown in Figure 18. The wall damping formulation has larger values of eddy viscosity than the local damping, with the peak values in eddy viscosity 37% higher with wall damping. The crossover point between the inner and outer layer formulations occurs at about the same location with local damping and wall damping, but the wall damping eddy viscosity is already 33% above the local damping value at that point.

These results show a growing difference between the CFD predictions with local damping and wall damping as T_w/T_t or H_w/H_t is decreased. In all cases, the local damping predictions had good or reasonable agreement with the experimental heating data, while the wall damping predictions were at least 25% above the data. In the lowest T_w/T_t case, the wall damping predictions were 39% higher than the data. The local damping predictions had reasonable or fair agreement with the experimental skin friction data, and again the wall damping predic-

tions were at least 22% above the data. A 30% overprediction of turbulent heating and skin friction will adversely affect the TPS sizing and drag estimates for the Hyper-X flight vehicles. These results show the importance of temperature gradient effects in turbulence modeling for hypersonic flows.

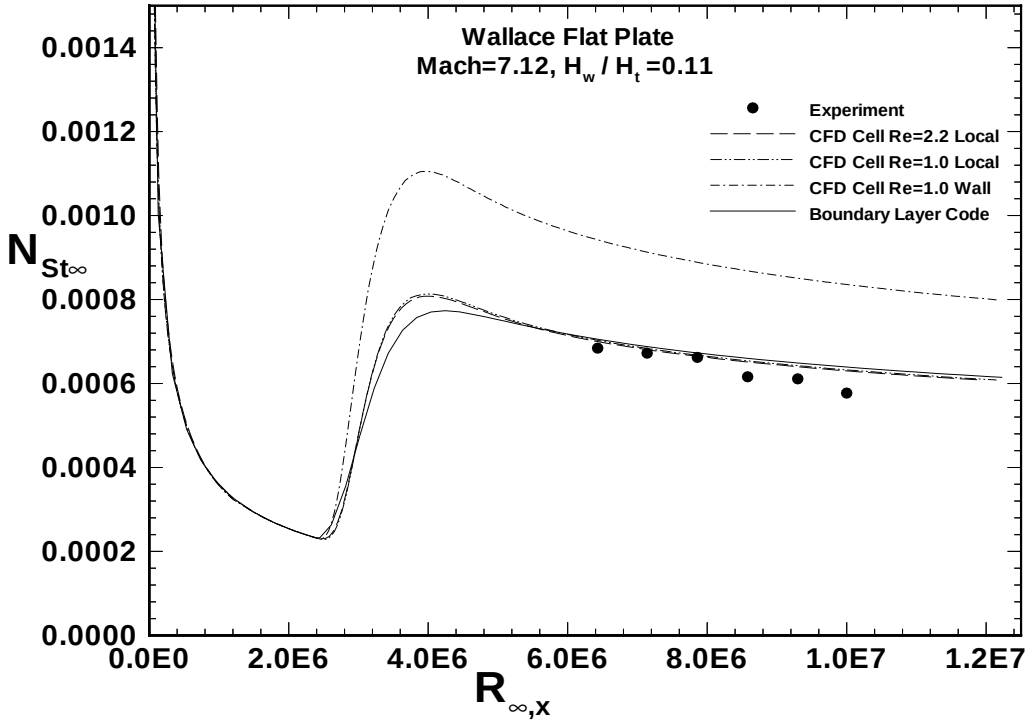

Figure 8. Mach 7.12 Heating Comparisons

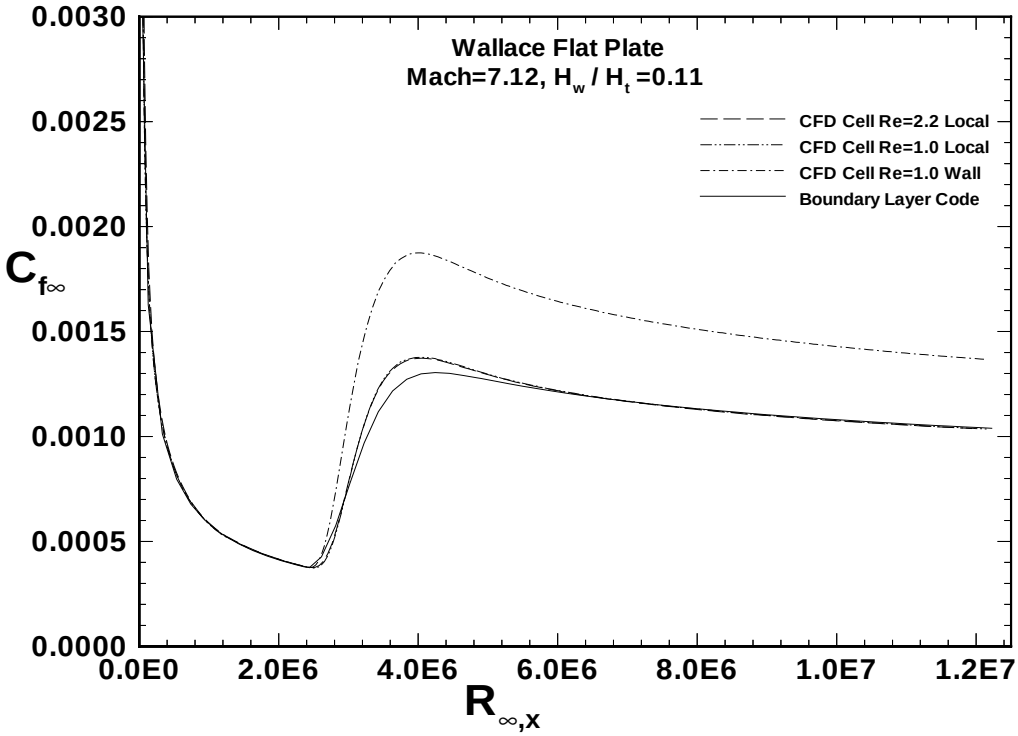

Figure 9. Mach 7.12 Skin Friction Comparisons

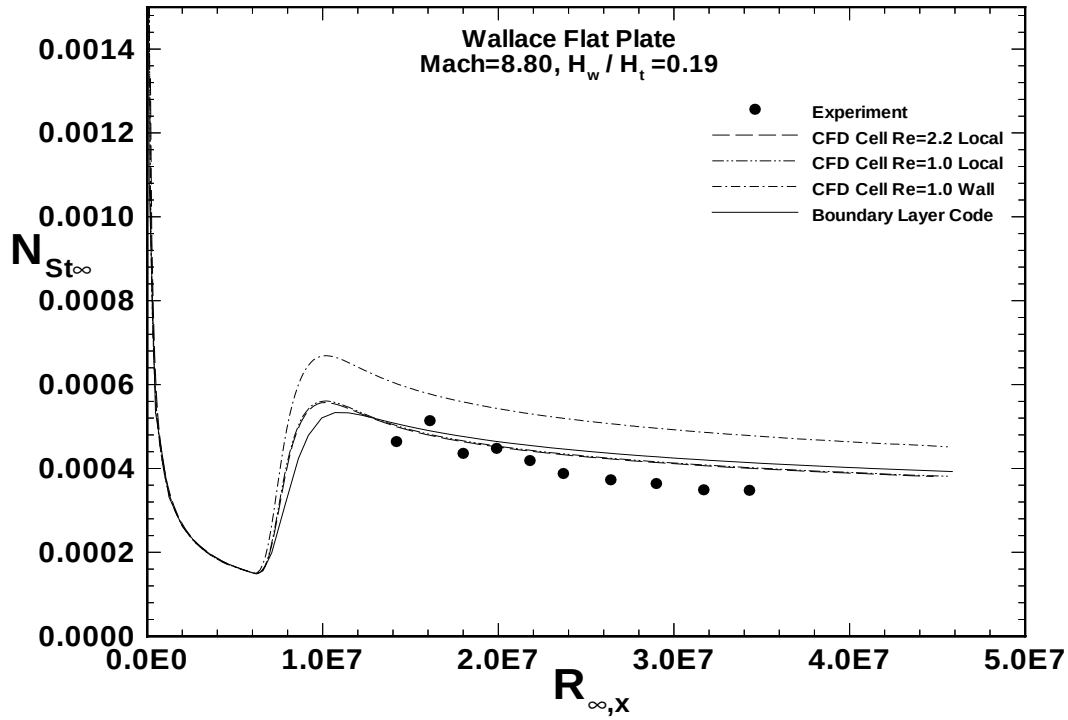

Figure 10. Mach 8.80 Heating Comparisons

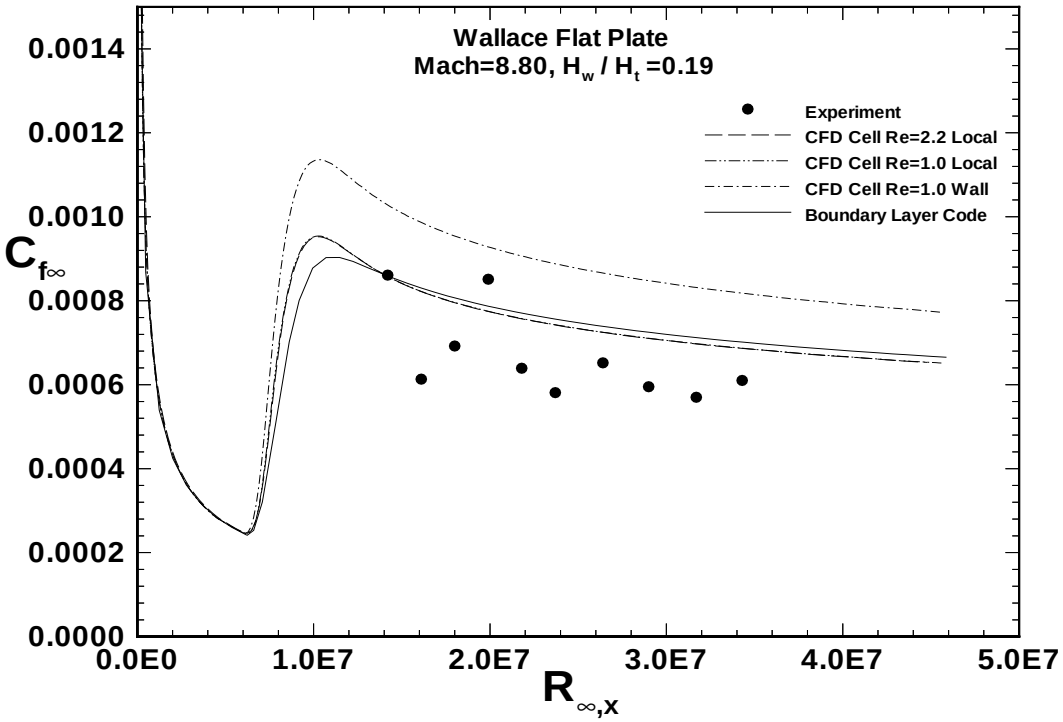

Figure 11. Mach 8.80 Skin Friction Comparisons

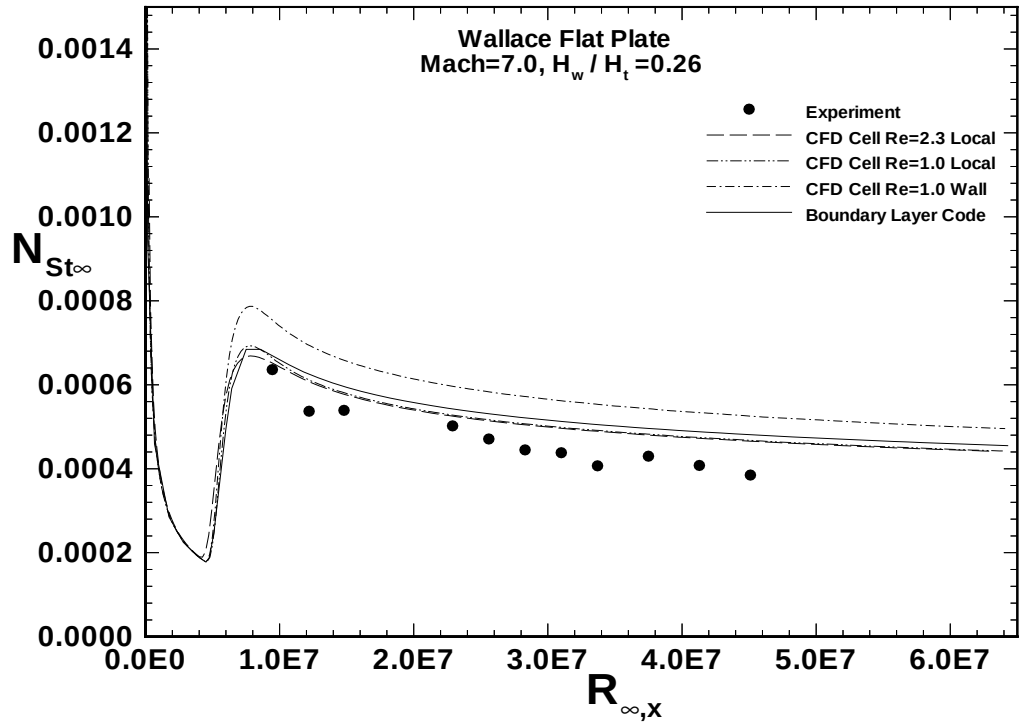

Figure 12. Mach 7.0 Heating Comparisons

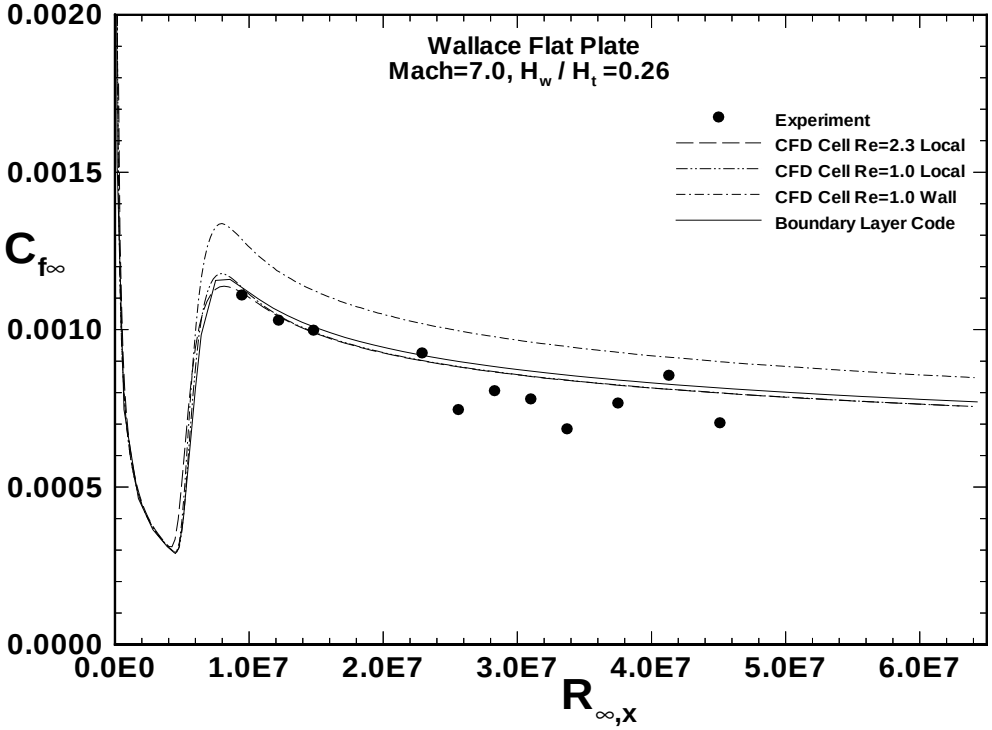

Figure 13. Mach 7.0 Skin Friction Comparisons

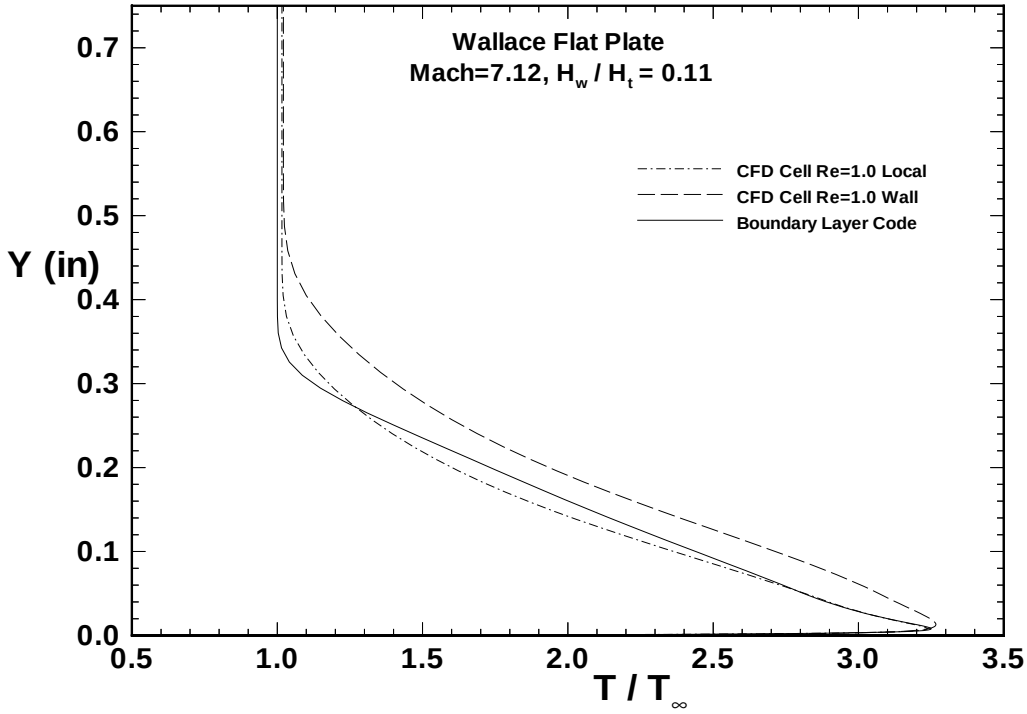

Figure 14. Mach 7.12 Temperature Profiles at 29.4"

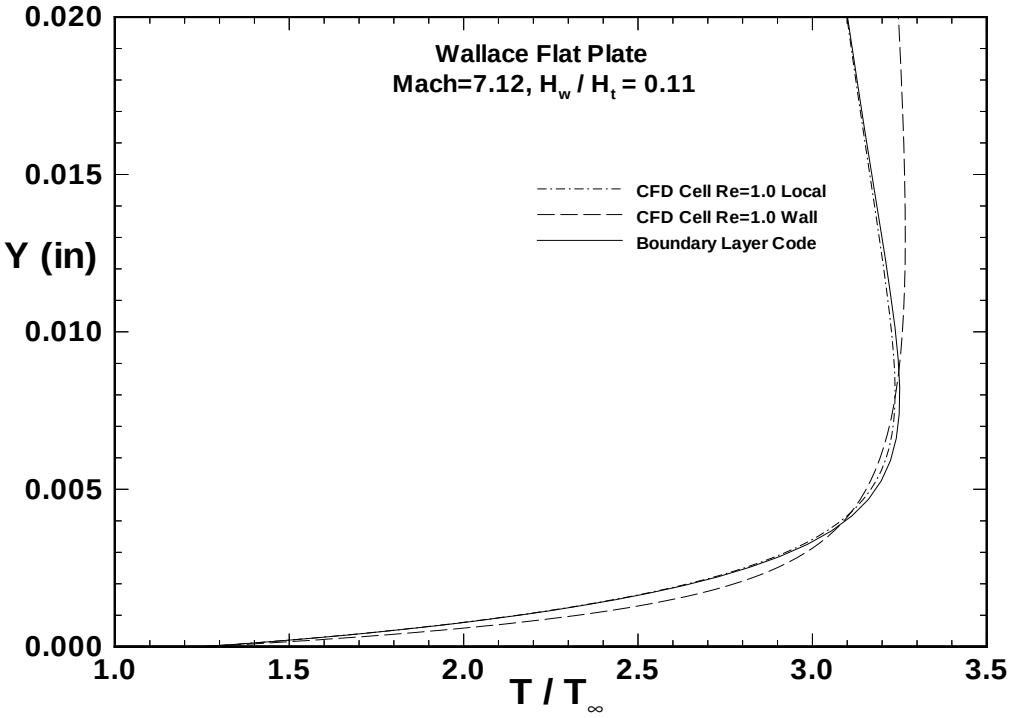

Figure 15. Mach 7.12 Temperature Profiles Near the Surface

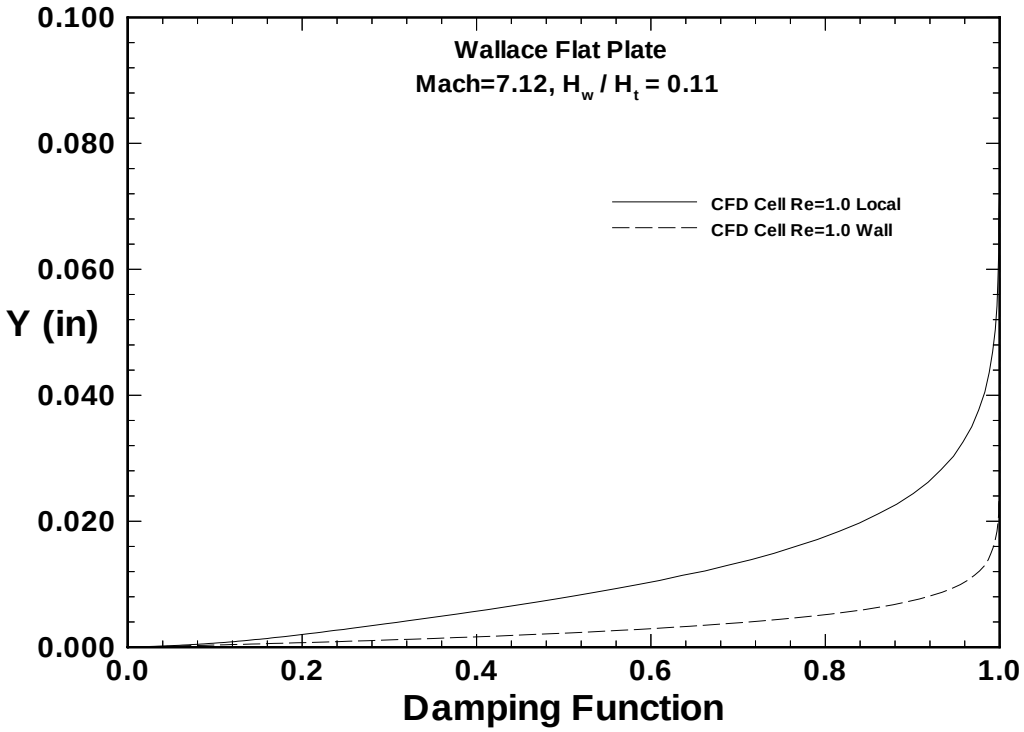

Figure 16. van Driest Damping Function with Local and Wall Damping

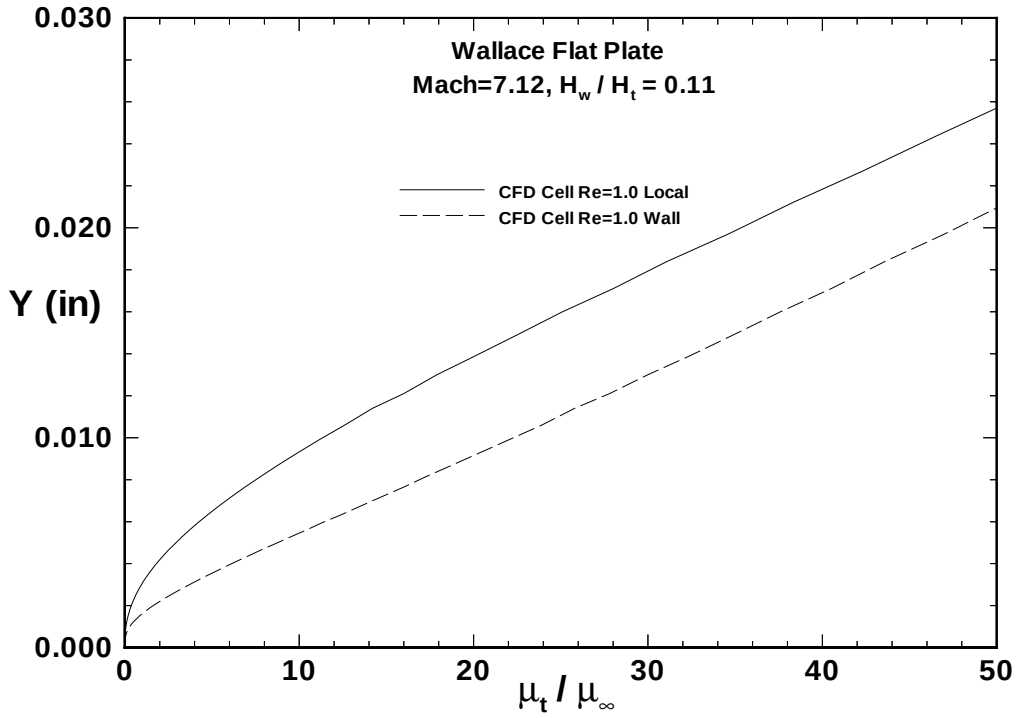

Figure 17. Turbulent Eddy Viscosity Profiles Near the Surface

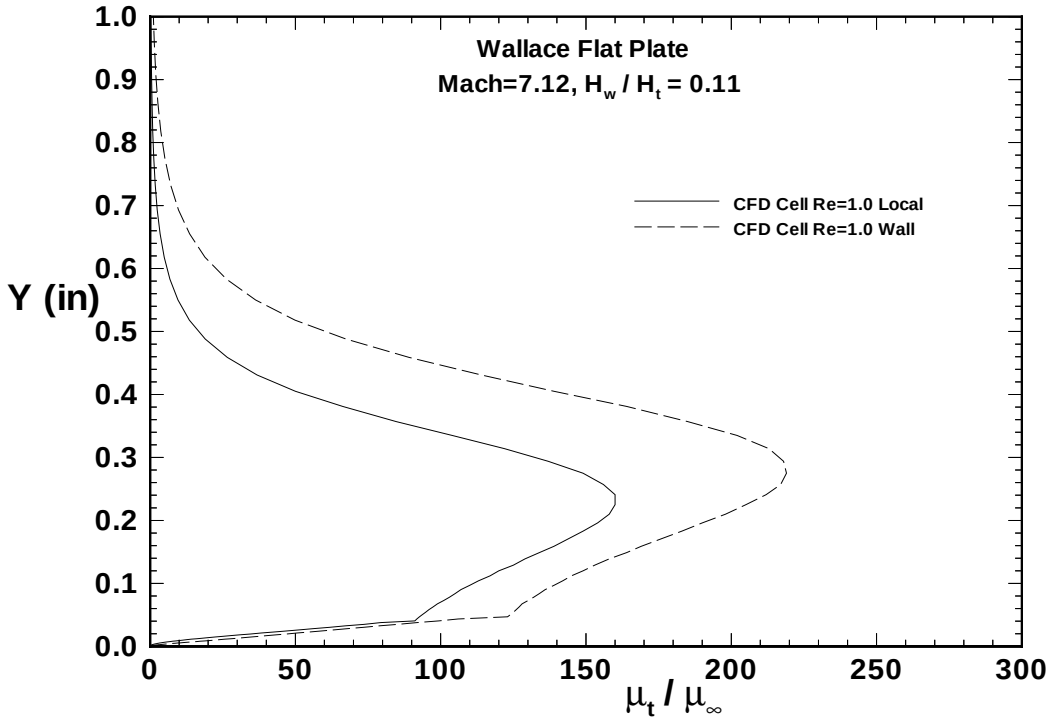

Figure 18. Mach 7.12 Turbulent Eddy Viscosity Profiles

5.4 Computational Requirements for Accurate Heating Predictions

The cold wall cases required a Re_{cell} of 2 for grid converged solutions, while the hot wall cases required a Re_{cell} of 1. However, these computational grids are not practical for analyzing large scale hypersonic vehicles because of the fine normal and axial grid spacings. To assess the accuracy requirements for CFD turbulent heating predictions, coarser grids were used to compute the flowfields for the Wallace Mach 7.12 and the Bertram, Cary and Whitehead T_w/T_t=0.6 cases. The grid dimensions and spacings, and Re_{cell}, y^+ and number of points in the boundary layer are given in Table 4, with the grids numbered from the coarsest to the finest. The percentage change from the turbulent heating levels with the finest grid are given in the last column. In both cases, the coarsest grid has less than 20% of the total grid points of the finest grid and 30% of the grid points in the boundary layer. The results for the Wallace case are shown in Figures 19-22. The heating predictions in Figure 19 show a 5.8% difference with grid 1 and a 2.8% difference with grid 2. The skin friction results in Figure 20 show a smaller change, with the grid 1 results 1.8% below the finest grid. The temperature profiles at the last axial station in Figure 21 have excellent agreement. The symbols at each cell center also show the refinement of the grid was concentrated near the surface, while the grid near the boundary layer edge had much less refinement. The temperature profiles in Figure 22 show small differences at the surface due to the coarsening. The y^+ of the coarsest grid satisfies Fletcher's recommendation[10] of y^+ less than 2. The results for the Bertram, Cary and Whitehead case are shown in Figures 23-26. The heating predictions in Figure 23 have a 5.7% difference with grid 1 and a 2.9% difference with grid 2. The skin friction results in Figure 24 again have a smaller change, with grid 1 results differing by 0.7% from the finest grid. As in the previous case, the temperature profiles at the last axial station in Figures 25 and 26 have excellent agreement. In this case, the y^+ of the coarsest grid is smaller than with the cold wall. These results indicate that while a Re_{cell}=1.0 may be required for grid converged heating predictions for these flat plate cases, this requirement is overly restrictive for design activities. For design purposes, a 6% underprediction in heating levels is acceptable and the reduction in computational time with the smaller grids enhances the overall efficiency of the analysis. Because of the limited nature of this study, this conclusion is limited to sharp nose geometries, and blunt geometries with a localized stagnation point may require a Re_{cell}=1.0.

Table 4. Heating Prediction Accuracy Requirement Cases

Case Description	Grid	Re_{cell}	y_1^+	# pts	Grid Dimensions	Δy_1 (in)	Δx_{max} (in)	ΔN_{St_∞}
Wallace	1	17.2	1.46	37	81 x 91	$.50x10^{-3}$	.502	5.8%
Mach 7.12	2	9.4	0.77	52	101 x 121	$.24x10^{-3}$	.335	2.8%
H_w / H_t = 0.11	3	1.0	0.08	126	201 x 321	$.23x10^{-4}$	.100	-
Bertram, Cary and Whitehead	1	7.1	0.47	35	61 x 81	$.60x10^{-3}$	.3455	5.7%
	2	3.6	0.23	51	81 x 101	$.30x10^{-3}$	.2255	2.9%
Mach 6	3	0.5	0.03	120	161 x 191	$.38x10^{-4}$	.1000	-
T_w / T_t = 0.6								

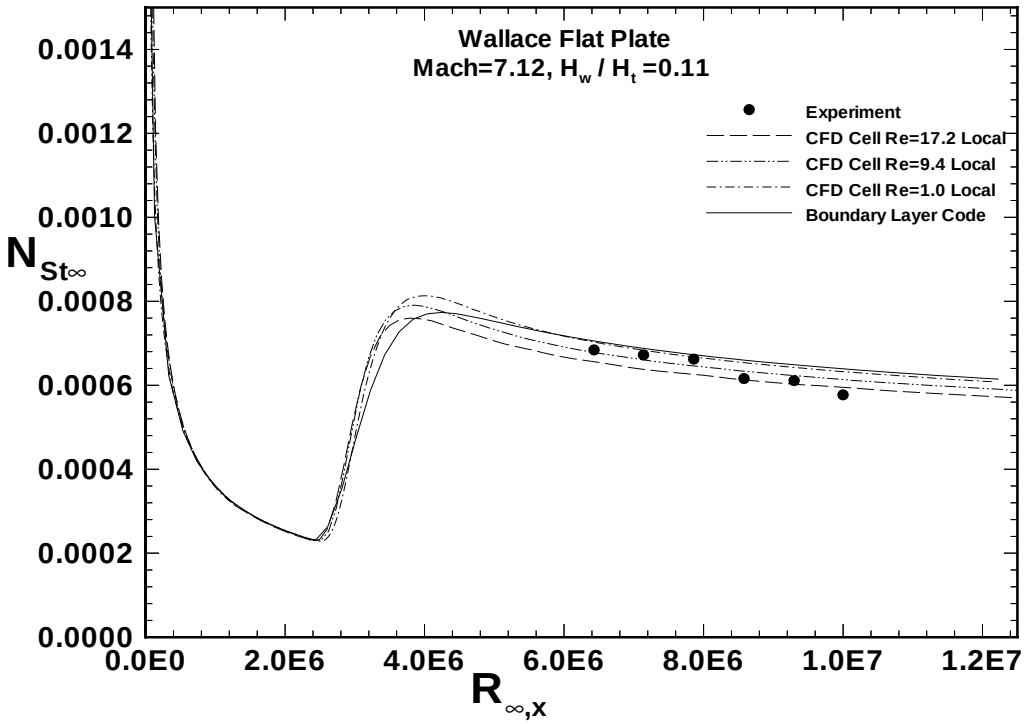

Figure 19. Mach 7.12 Heating Comparisons with Coarser Grids

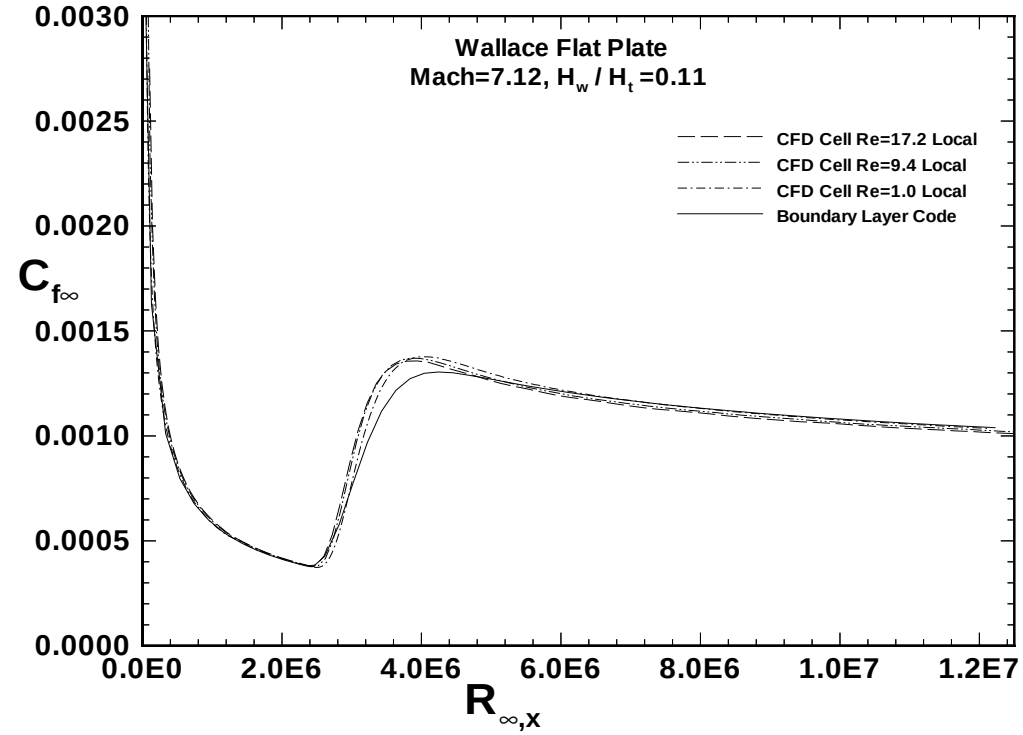

Figure 20. Mach 7.12 Skin Friction Comparisons with Coarser Grids

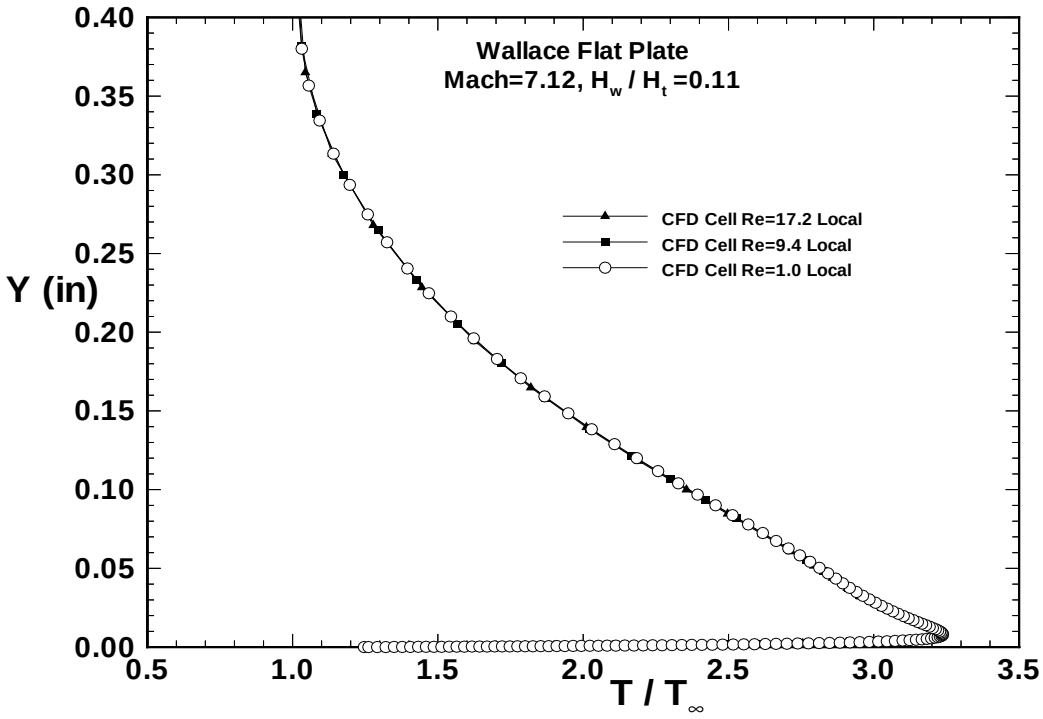

Figure 21. Mach 7.12 Temperature Profiles with Coarser Grids

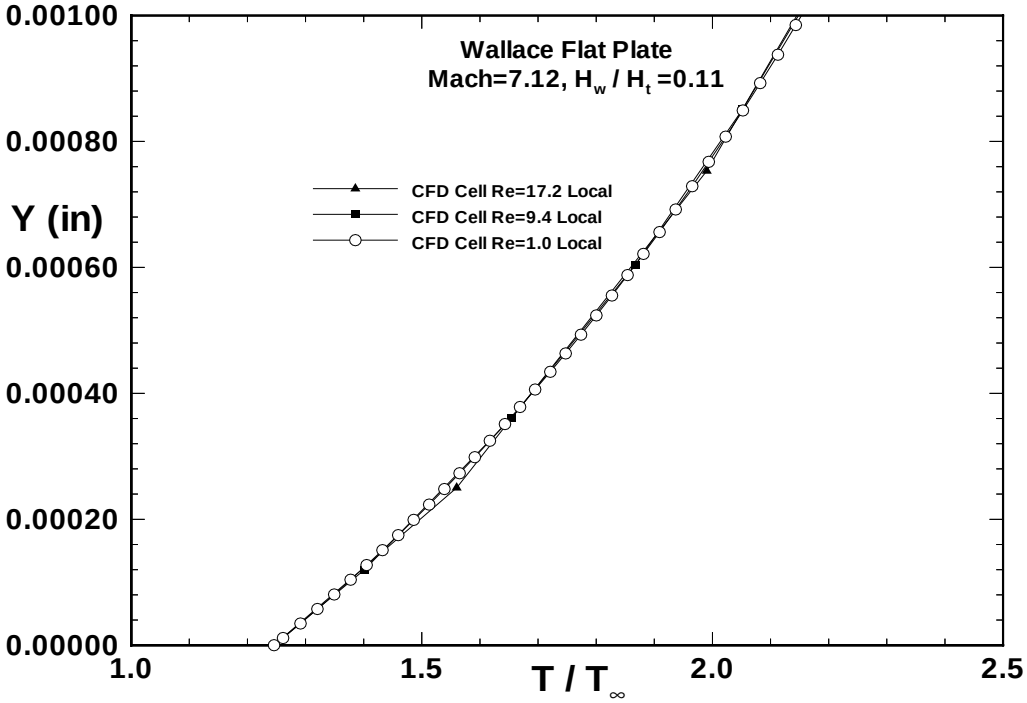

Figure 22. Mach 7.12 Temperature Profiles Near the Surface

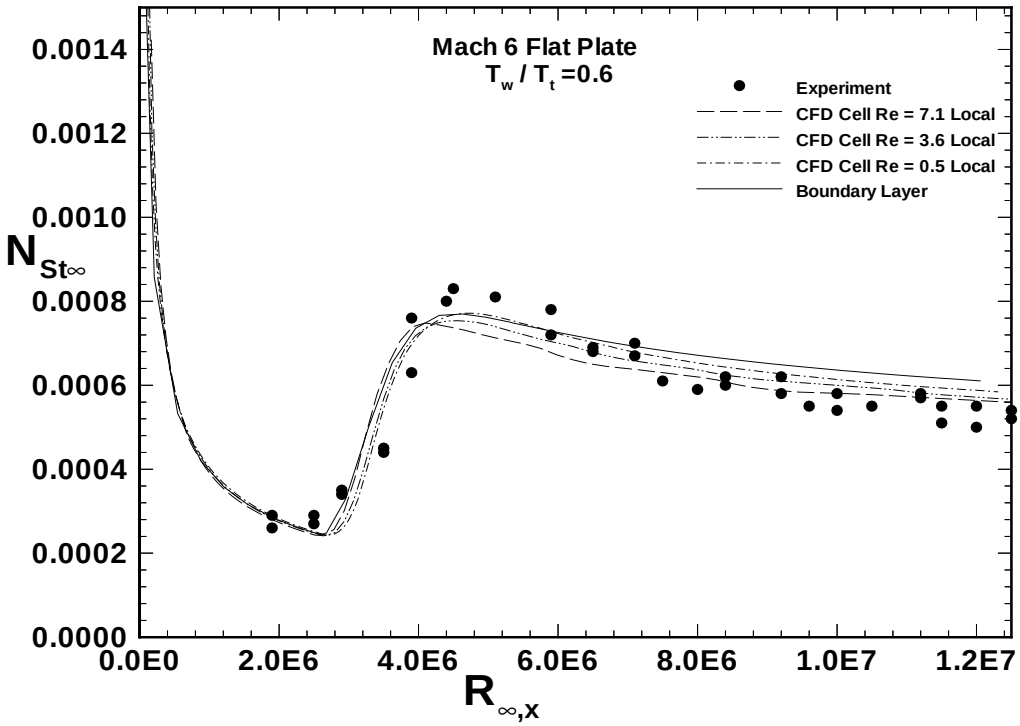

Figure 23. Mach 6 Heating Comparisons with Coarser Grids

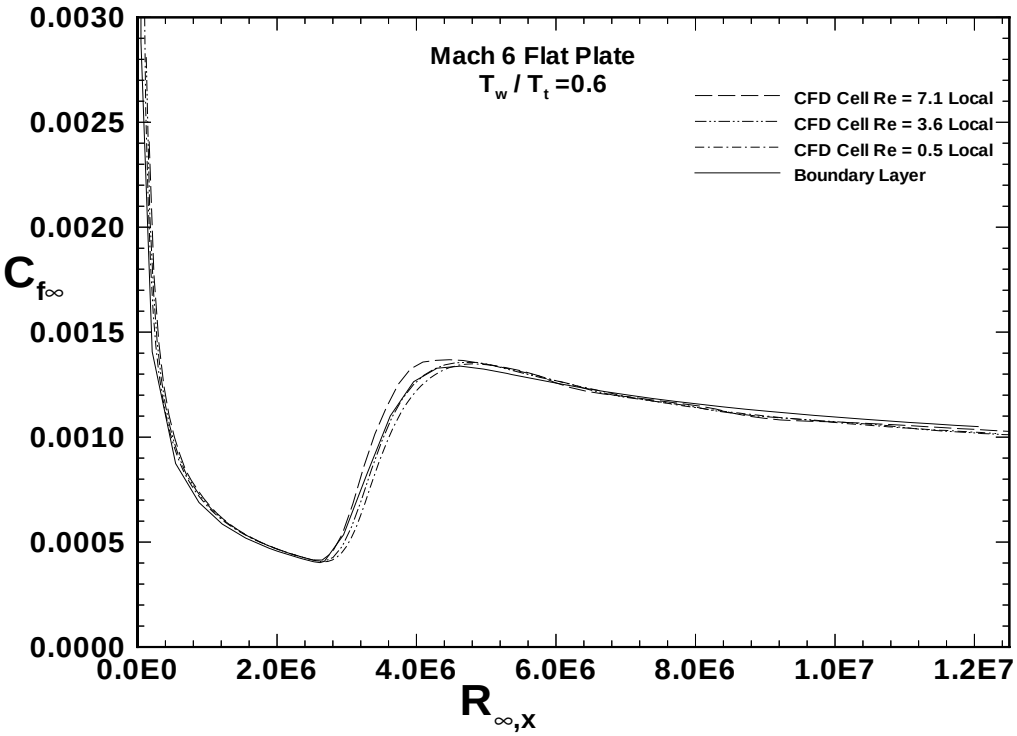

Figure 24. Mach 6 Skin Friction Comparisons with Coarser Grids

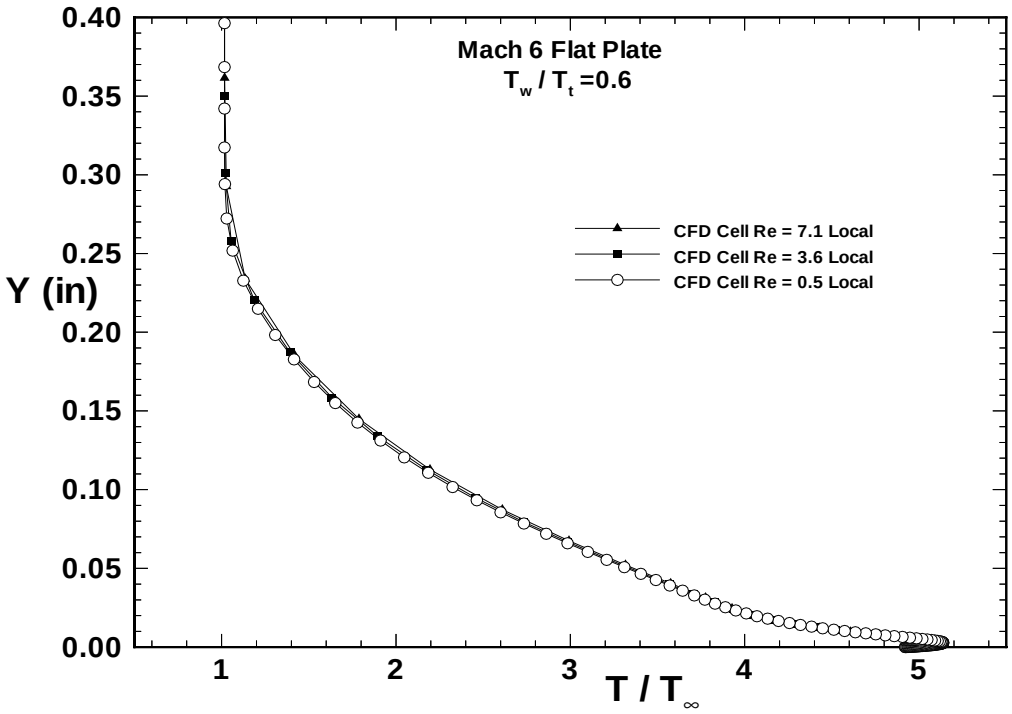

Figure 25. Mach 6 Temperature Profiles with Coarser Grids

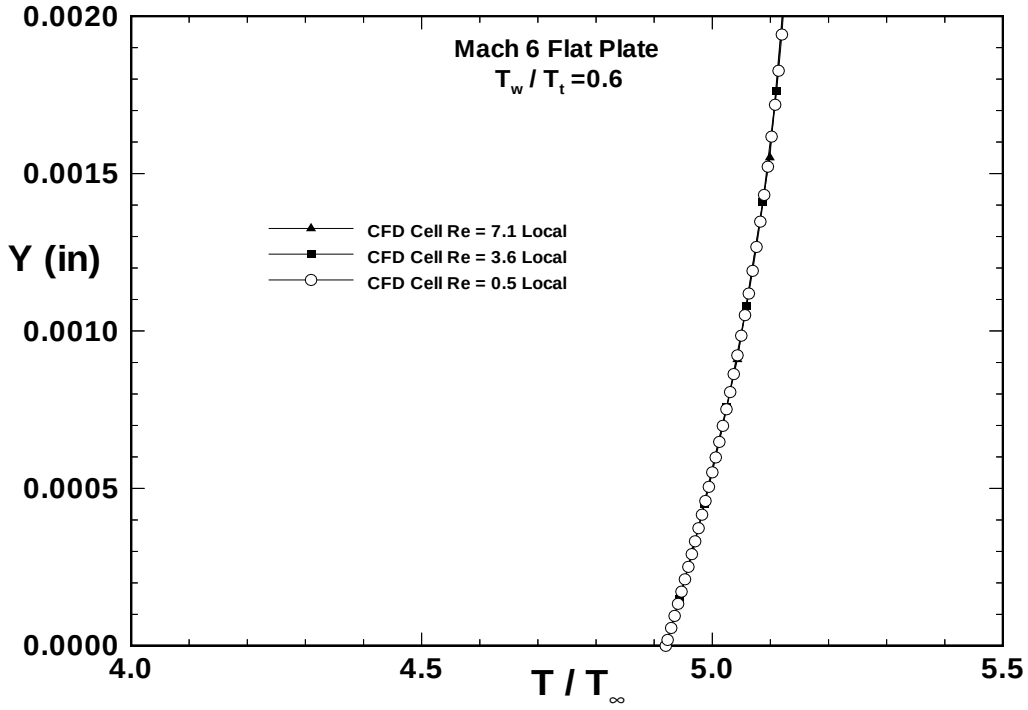

Figure 26. Mach 6 Temperature Profiles Near the Surface

6. Conclusions

Results from a study to assess the accuracy of CFD turbulent heating and skin friction prediction techniques for hypersonic applications have been presented. The study used the original and a modified Baldwin-Lomax turbulence model with a PNS code. Grid converged turbulent predictions using the wall damping formulation (original model) and local damping formulation (modified model) were compared with experimental data for several flat plates. The wall damping and local damping results were similar for hot wall conditions, but differed significantly for cold walls with the wall damping heating and skin friction 10-30% above the local damping values. Furthermore, the local damping predictions had reasonable or good agreement with the experimental heating data and reasonable or fair agreement with the experimental skin friction data. The impact of the two damping formulations on the van Driest damping function and the turbulent eddy viscosity distribution was shown for a cold wall case, indicating the importance of temperature gradient effects. Grid requirements for accurate turbulent heating predictions were also studied by using coarser grids to obtain predictions for a cold wall and a hot wall case. These results indicated that a cell Reynolds number of 1 may be required for grid converged solutions, but coarser grids are adequate for design purposes. The cold wall results supported the less restrictive requirement of y^+ less than 2.

The comparisons between CFD predictions and experimental data presented in this report are for hypersonic flat plate flowfields. In all cases, the local damping formulation had as good or better agreement with the data than the wall damping. At the cold wall conditions, the wall damping overpredicted the turbulent heating data by as much as 40%. Therefore, it is recommended that the local damping formulation be used with the Baldwin-Lomax and Cebeci-Smith turbulence models for design and analysis of the Hyper-X flight vehicles. Because the Hyper-X design uses forebody compression surfaces on the engine flowpath, further study is required to determine the impact of local damping and wall damping in regions of isentropic and discrete compression. But given the current results, the use of local damping with algebraic turbulence models is recommended for obtaining accurate turbulent heating and skin friction predictions.

7. References

1). Rausch, V. L., McClinton, C. R. and Hicks, J. W., "NASA Scramjet Flights to Breath New Life into Hypersonics," *Aerospace America*, July 1997.

2). Walters, R. W., Reu, T., McGrory, W. D., Thomas, J. L. and Richardson, P. F., "A Longitudinally-Patched Grid Approach With Applications to High Speed Flows," AIAA Paper 88-0715.

3). Baldwin, B. S. and Lomax, H., "Thin-Layer Approximation and Algebraic Model for Separated Turbulent Flows," AIAA Paper 78-0257.

4). Shirazi, S. A. and Truman, C. R., "Comparison of Algebraic Turbulence Models for PNS Predictions of Supersonic Flow Past a Sphere-Cone," AIAA Paper 87-0544.

5). Voung, S. T. and Coakley, T. J., "Modeling of Turbulence for Hypersonic Flows With and Without Separation," AIAA Paper 87-0286.

6). Cebeci, T. and Smith, A. M. O.: **Analysis of Turbulent Boundary Layers**, Academic Press, New York, New York,1974, pp. 215-217, 256, 264.

7). Stock, H. W. and Haase, W.: "Determination of Length Scales in Algebraic Turbulence Models for Navier-Stokes Methods," *AIAA Journal*, Vol. 27, No. 1, 1989, pp. 5-14.

8). Cheatwood, F. N. and Thompson, R. A.: "The Addition of Algebraic Turbulence Modeling to Program LAURA," NASA TM-107758, April 1993.

9). Weilmuenster, K. J. and Gnoffo, P. A.: "Solution Strategy for Three-Dimensional Configurations at Hypersonic Speeds," *Journal of Spacecraft and Rockets*, Vol. 30, No. 4, 1993, pp. 385-394.

10). Fletcher, C. A. J.: **Computational Techniques for Fluid Dynamics**, 2nd ed., Vol II, Springer-Verlag, Berlin, 1991, pp. 404-406.

11). Huebner, L. D., Pittman, J. L. and Dilley, A. D.: "Hypersonic Parabolized Navier-Stokes Code Validation on a Sharp-Nose Cone," *Journal of Aircraft*, Vol. 26, No. 7, 1989, pp. 650-656.

12). Huebner, L. D. and Haynes, D. A.: "Forebody Redesign and Flow Characterization of the Test Technique Demonstrator at Mach 6," NASA TP-1013, April 1994.

13). Richardson, P. F., Parlette, E. B., Morrison, J. H., Switzer, G. F., Dilley, A. D. and Eppard, W. M.: "Comparison Between Experimental and Numerical Results for a Research Hypersonic Aircraft," *Journal of Aircraft*, Vol. 27, No. 4, 1990, pp. 300-305.

14). Dilley, A. D., Switzer, G. F. and Eppard, W. M.: "Zonal Analysis of Two High-Speed Inlets," *Computational Fluid Dynamics Symposium on Aeropropulsion*, NASA CP-3078, April 1990, pp. 507-519.

15). Dhawan, S. and Narasimha, R.: "Some Properties of Boundary Layer Flows During the Transition from Laminar to Turbulent Motion," *Journal of Fluid Mechanics*, Vol. 3, No. 4., 1958, pp. 418-436.

16). Anderson, E. C. and Lewis, C. H.: "Laminar or Turbulent Boundary-Layer Flows of Perfect Gases or Reacting Gas Mixtures in Chemical Equilibrium," NASA CR-1893, Oct. 1971.

17). Bertram, M. H., Cary Jr., A. M., and Whitehead Jr., A. H.: "Experiments With Hypersonic Turbulent Boundary Layers on Flat Plates and Delta Wings," *AGARD Specialists' Meeting on Hypersonic Boundary Layers and Flow Fields*, London, England, May 1968.

18). Bertram, M. H. and Neal Jr., L.: “Recent Experiments in Hypersonic Turbulent Boundary Layers,” *AGARD Specialists’ Meeting on Recent Developments in Boundary Layer Research*, Naples, Italy, May 1965.

19). Wallace, J. E.: “Hypersonic Turbulent Boundary Layer Studies at Cold Wall Conditions,” *Proceedings of the 1967 Heat Transfer and Fluid Mechanics Institute*, Paul A. Libby, Daniel B. Olfe and Charles W. Van Atta, eds, Stanford University Press, 1967, pp. 427-451.

REPORT DOCUMENTATION PAGE

Form Approved
OMB No. 0704-0188

1. AGENCY USE ONLY *(Leave blank)*	2. REPORT DATE	3. REPORT TYPE AND DATES COVERED
	March 2001	Contractor Report

4. TITLE AND SUBTITLE
Evaluation of CFD Turbulent Heating Prediction Techniques and Comparison With Hypersonic Experimental Data

5. FUNDING NUMBERS
C NAS1-00135

WU 522-51-21-10

6. AUTHOR(S)
Arthur D. Dilley

7. PERFORMING ORGANIZATION NAME(S) AND ADDRESS(ES)
Swales Aerospace
NASA Langley Research Center, MS 186A
1224 T-11 Wright St.
Hampton, VA 23681-2199

8. PERFORMING ORGANIZATION REPORT NUMBER

9. SPONSORING/MONITORING AGENCY NAME(S) AND ADDRESS(ES)
National Aeronautics and Space Administration
Langley Research Center
Hampton, VA 23681-2199

10. SPONSORING/MONITORING AGENCY REPORT NUMBER
NASA/CR-2001-210837

11. SUPPLEMENTARY NOTES
Langley Technical Monitor: Charles R. McClinton

12a. DISTRIBUTION/AVAILABILITY STATEMENT
Unclassified–Unlimited
Subject Category 02 Distribution: Nonstandard
Availability: NASA CASI (301) 621-0390

12b. DISTRIBUTION CODE

13. ABSTRACT ***(Maximum 200 words)***

Results from a study to assess the accuracy of turbulent heating and skin friction prediction techniques for hypersonic applications are presented. The study uses the original and a modified Baldwin-Lomax turbulence model with a space marching code. Grid converged turbulent predictions using the wall damping formulation (original model) and local damping formulation (modified model) are compared with experimental data for several flat plates. The wall damping and local damping results are similar for hot wall conditions, but differ significantly for cold walls, i.e. $T_w / T_t < 0.3$, with the wall damping heating and skin friction 10-30% above the local damping results. Furthermore, the local damping predictions have reasonable or good agreement with the experimental heating data for all cases. The impact of the two formulations on the van Driest damping function and the turbulent eddy viscosity distribution for a cold wall case indicate the importance of including temperature gradient effects. Grid requirements for accurate turbulent heating predictions are also studied. These results indicate that a cell Reynolds number of 1 is required for grid converged heating predictions, but coarser grids with a y^+ less than 2 are adequate for design of hypersonic vehicles. Based on the results of this study, it is recommended that the local damping formulation be used with the Baldwin-Lomax and Cebeci-Smith turbulence models in design and analysis of Hyper-X and future hypersonic vehicles.

14. SUBJECT TERMS	15. NUMBER OF PAGES
CFD, Turbulence Modeling, Hypersonics	31
	16. PRICE CODE A03

17. SECURITY CLASSIFICATION OF REPORT	18. SECURITY CLASSIFICATION OF THIS PAGE	19. SECURITY CLASSIFICATION OF ABSTRACT	20. LIMITATION OF ABSTRACT
Unclassified	Unclassified	Unclassified	UL